8 $^{40}Ar/^{39}Ar$ thermochronological constraints on the retrogression and exhumation of the ultra-high pressure metamorphic rocks of the Xitieshan terrane, North Qaidam*

8.1 Introduction

The $^{40}Ar/^{39}Ar$ method is commonly applied to derive age information on metamorphic rocks. Based on different minerals with different closure temperatures, $^{40}Ar/^{39}Ar$ thermo-chronological analyses provide critical constraints to quantify temperature-time (*T-t*) paths for metamorphic rocks (Hacker and Wang, 1995; McDougall and Harrison, 1999; Di Vincenzo and Palmeri, 2001; Hacker et al., 2003; Webb et al., 2006; Wilke et al., 2010; Warren et al., 2014). Consequently, the tectonothermal evolution and exhumation rates of an orogenic crust can be better understood when the $^{40}Ar/^{39}Ar$ dating method is combined petrologic and geothermobarometrical studies.

In the North Qaidam Orogen, geochronological studies have mainly focused on the timing of the peak eclogite facies metamorphism on the basis of U-Pb zircon dating (Mattinson et al., 2007; Liu et al., 2012; Song et al., 2014). Several studies have applied $^{40}Ar/^{39}Ar$ dating to the northwestern portion of this belt (Yuka and Luliangshan terranes, Zhang et al., 2005a; Menold, 2006; Hu et al., 2013), whereas in the central segment (Xitieshan terrane), $^{40}Ar/^{39}Ar$ data are rather limited. The mechanism and path of exhumation of the ultrahigh pressure rocks in this area remains unresolved partly due to the lack of appropriate age constraints on the retrograde history.

In this chapter, laser stepwise $^{40}Ar/^{39}Ar$ dating has been applied to amphibole, muscovite, biotite and K-feldspar from garnet-amphibolite, amphibolite, schist and gneiss samples collected in the Xitieshan terrane. The new $^{40}Ar/^{39}Ar$ results were used to assess the timing of retrograde petrogenetic processes at different *P-T* conditions. Combining these new data with published zircon U-Pb data (Zhang et al., 2005a; Zhang et al., 2011a; Liu et al., 2012) and information about the local *P-T-t* evolution (Zhang et al., 2011a), allows estimation of rates of cooling and exhumation for the Xitieshan HP/UHP rocks from upper-mantle to upper-crustal depths.

8.2 Geological setting and previous age constraints in the Xitieshan terrane

The North Qaidam HP/UHP metamorphic belt, situated in the northern edge of the Tibet Plateau, NW China, is bounded by the Qilian block to the northeast and the Qaidam block to the southeast. The Qilian block consists of Precambrian gneiss, schist, marble, amphibolite and minor granulite which was overlain by Neoproterozoic-Paleozoic

* This chapter was not part of the Chinese version of the thesis.

sedimentary rocks (Wan et al., 2001). The Qaidam block is a Mesozoic-Cenozoic intra-continental basin with up to 10 km of Jurassic to Quaternary sediments underlain by Precambrian crystalline basement and a Paleozoic fold belt (BGMQ., 1991).

The Xitieshan terrane is located in the central segment of the North Qaidam Orogen (Figure 8.1a). It mainly consists of paragneiss and granitic orthogneiss of the Dakendaban Group, and was intruded by granite plutons dated at 428 ± 1 Ma (Meng et al., 2005). Eclogites generally occur as lenses or boudins incorporated within gneisses, and commonly intensely overprinted by garnet-granulite, garnet-amphibolite or amphibolite mineral associations (Yang et al., 2002b; Zhang et al., 2005a).

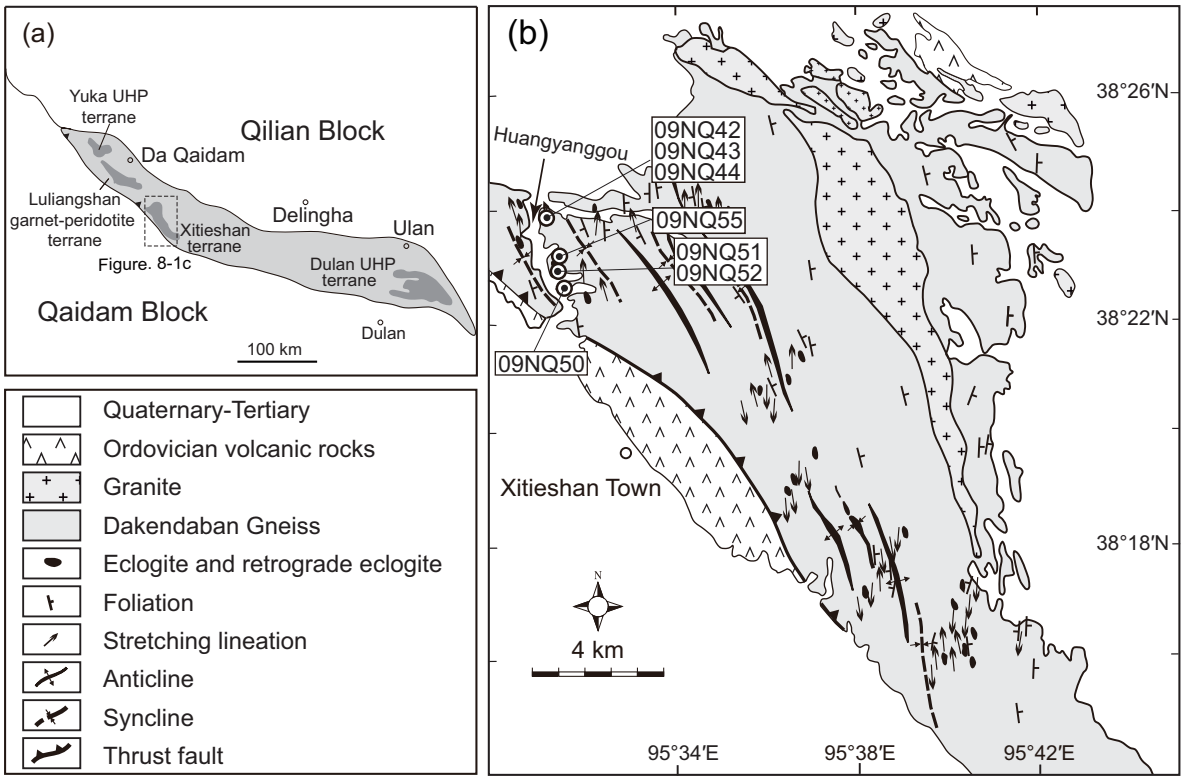

Figure 8.1 Regional map of the Xitieshan terrane and studied samples localities. Modified from (Zhang et al., 2005a).

Thermobarometric and geochronological studies show evidence that eclogites and their country rock gneisses in Xitieshan area underwent early Paleozoic HP/UHP metamorphism as an integral block and thus share a common history (Zhang et al., 2006; Zhang et al., 2012). Peak eclogite-facies *P-T* conditions of *P* = 27.1 – 31.7 kbar, *T* = 750 – 790 °C for Xitieshan eclogites were obtained using the Garnet–Omphacite–Phengite geo-thermobarometer (Zhang et al., 2011a). No eclogite-facies mineral assemblages have been recognized in the country rocks in this terrane so far (Zhang et al., 2008a; Zhang et al., 2011a). Geo-thermobarometry and phase equilibrium calculations suggest *P-T* conditions of 4.6 – 8.6 kbar and 560 – 800 °C for the Xitieshan pelitic gneisses, indicating these have experienced granulite- to upper amphibolite-facies metamorphism (Zhang et al., 2008a; Zhang et al., 2012).

Table 8.1 Published geochronological data for the Xitieshan UHP terrane

Rock type	Method	Age (Ma, ± 2σ)	Interpretation	Author(s)
eclogite	U-Pb Zrn SHRIMP	480 ± 16	Peak metamorphism	Zhang JX et al. (2005a)
granite	U-Pb Zrn TIMS	428 ± 1	Magmatic crystallization	Meng FC et al.(2005)
paragneiss	U-Pb Zrn SHRIMP	437 ± 6	MP granulite-facies metamorphism	Zhang JX et al. (2008b)
paragneiss	U-Pb Zrn SHRIMP	441 ± 15	MP granulite-facies metamorphism	Zhang JX et al. (2008b)
paragneiss	U-Pb Zrn SHRIMP	461 ± 8	HP granulite-facies metamorphism	Zhang JX et al. (2009c)
paragneiss	U-Pb Zrn SHRIMP	451 ± 6	HP granulite-facies metamorphism	Zhang JX et al. (2009c)
paragneiss	U-Pb Zrn SHRIMP	423 ± 13	Amphibolite-facies metamorphism	Zhang JX et al. (2009c)
metabasite	U-Pb Zrn SHRIMP	452 ± 12	Peak metamorphism	Zhang JX et al. (2009c)
metabasite	U-Pb Zrn SHRIMP	430 ± 4	Retrograde metamorphism	Zhang JX et al. (2009c)
eclogite	U-Pb Zrn SHRIMP	439 ± 8	Peak metamorphism	Zhang C et al. (2011)
eclogite	U-Pb Zrn SHRIMP	461 ± 4	Peak metamorphism	Zhang C et al. (2011)
eclogite	U-Pb Zrn SHRIMP	440 ± 5	Peak metamorphism	Zhang C et al. (2011)
gneiss	EMP; Mon U-Th-Pb	460 ± 14	Prograde peak metamorphism	Zhang C et al. (2012)
gneiss	EMP; Mon U-Th-Pb	425 ± 14	Retrograde metamorphism	Zhang C et al. (2012)
eclogite	U-Pb Zrn SIMS	433 ± 3	Peak metamorphism	Song et al. (2011)
Coe-amphibolite	U-Pb Zrn SIMS	441 ± 7	Peak metamorphism	Liu et al.(2012)
Coe-amphibolite	U-Pb Zrn LA-ICPMS	432 ± 14	Peak metamorphism	Liu et al.(2012)
eclogite	U-Pb Zrn LA-ICPMS	458 ± 2	Peak metamorphism	Chen et al.,(2012)
felsic veins	U-Pb Zrn LA-ICPMS	428 ± 2	Veining	Chen et al.,(2012)
eclogite	Amp Ar-Ar	407 ± 4	Cooling	Zhang JX et al. (2005a)
gneiss	Ms Ar-Ar	405 ± 4	Cooling	Xu ZQ et al. (2006)

Geochronological results for the Xitieshan terrane are summarized in Table 8.1. Eclogite zircon rim U-Pb ages yield ages of 480 – 486 Ma determined using the TIMS and SHRIMP methods were first reported by Zhang et al. (2005a), and were interpreted to be related to eclogite-facies metamorphism. Recently, the age of 480 ± 16 Ma from the SHRIMP method was recalculated to 466 ± 33 Ma by Liu et al. (2012), after excluding one analysis which had a substantially higher U and Th contents than the others. Metamorphic zircon grains from a metabasite yielded two weighted mean ages of 452 ± 12 and 430 ± 4 Ma by SHRIMP dating, which were interpreted as the timing of HP granulite-facies and amphibolite-facies metamorphism, respectively (Zhang et al., 2009c). It has also been suggested that the approximately 433 Ma old zircon U-Pb SIMS age from a Quanjixia eclogite represents the age of eclogite-facies metamorphism (Song et al., 2011). More recently, Zhang et al. (2011a) obtained zircon U-Pb ages ranging from 439 to 461 Ma for two eclogites by U-Pb SHRIMP dating, and interpreted these as representing the age of eclogite-facies metamorphism. Furthermore, two age groups of 460 ± 14 and 425 ± 14 Ma were obtained from three adjacent paragneisses on the basis of monazite EMP U-Th-Pb analyses. These ages were interpreted to be associated with prograde metamorphism and retrograde amphibolite-facies metamorphism, respectively (Zhang et al., 2012). Later, Chen et al. (2012) obtained a LA-ICPMS zircon U-Pb age of 458 ± 2 Ma for a felsic-vein bearing eclogite, and interpreted it as the timing of eclogite-facies metamorphism. Liu et al. (2012) reported two zircon U-Pb weight mean ages of 432 ± 14 Ma and 441 ± 9 Ma from a coesite-bearing amphibolite (coesite as inclusion in zircon) by using LA-ICPMS and SIMS methods, respectively, and the age of 441 ± 9 Ma was regarded as the age of peak UHP metamorphism.

To summarize, in spite of the many zircon U-Pb dates published so far, there is no consensus on the age of the peak ultra-high pressure metamorphism. After careful comparison and examination, Liu considered the SIMS dating result 441 ± 9 Ma to be the best estimate for the age of peak UHP metamorphism in the Xitieshan terrane (Liu et al., 2012). The reasons are the following: 1) Zircon grains for U-Pb dating were separated from retrogressed equivalents of coesite-bearing eclogite; 2) the results were identified using both the SIMS and LA-ICPMS methods.

There are only very few published amphibole and muscovite 40Ar/39Ar data from the Xitieshan terrane, and published ^{40}Ar/^{39}Ar chronology is currently limited to multi-grain stepwise heating data. Zhang et al. (2005a) reported an amphibole ^{40}Ar/^{39}Ar isochron age of 407 ± 4 Ma for a retrograde eclogite obtained by stepwise heating. Subsequently, Xu et al. (2006) reported a muscovite ^{40}Ar/^{39}Ar isochron age of 405 ± 4 Ma for mylonitic gneiss. Both these ages were interpreted as cooling ages.

8.3 Sample description and mineral chemistry

Seven samples were collected from the Huangyanggou area of the Xitieshan terrane for ^{40}Ar/^{39}Ar dating: a garnet-amphibolite (09NQ44), two amphibolites (09NQ43 and 09NQ50), a schist (09NQ42) and three gneisses (09NQ51, 52 and 55). Sample locations are shown in Figure 8.1b.

The garnet-amphibolite (09NQ44) contains mainly garnet, amphibole, plagioclase, and symplectites of clinopyroxene + plagioclase and amphibole + plagioclase, and is characterized by an intensive granulite- to upper amphibolite facies overprinting of an earlier eclogite facies mineral assemblage. Amphibole is the major phase in this sample. The amphibole generally can be divided into three types based on their petrographic positions and shows little compositional variation within each group. The first type (Amp-I) that occurs as inclusions in garnet, is classified as tschermakite. The second type (Amp-II) that occurs as a constituent of symplectite surrounding garnet is magnesio-hornblende and actinolite. The third type (Amp-III) is used for ^{40}Ar/^{39}Ar dating in this study and occurs as porphyroblasts in the matrix. It is classified as magnesio-hornblende, with mean K_2O content of ~3.8 wt.%, mean K/Ca and Fe/Mn ratios of ~0.04 and ~92, respectively (5 points, Table 8.2).

Plagioclase that is found within symplectite (Cpx + Pl or Amp-II + Pl) and in the matrix has similar general compositions of $Ab_{51-56}An_{44-47}Or_{0-1}$ (Table 8.3). Assuming local equilibrium between amphibole (Amp-III) and adjacent plagioclase (in matrix), the Amp-Pl geothermometer (Holland and Blundy, 1994) combined with the Amp-Pl-(Qz) geobarometer (Bhadra and Bhattacharya, 2007) reveals *P-T* conditions of 8.1 – 9.1 kbar and 630 – 670 °C, which would represent medium-pressure upper amphibolite-facies metamorphic conditions.

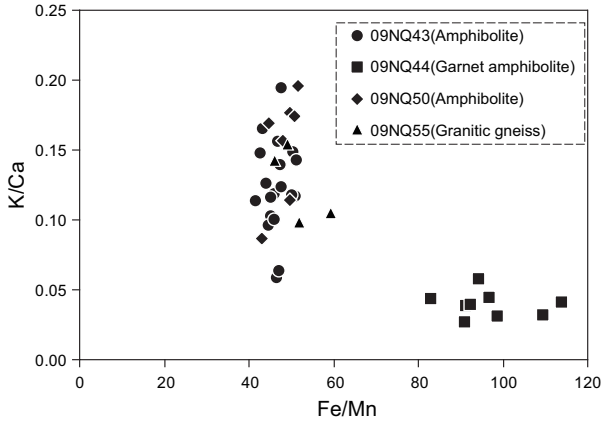

Figure 8.2 Amphibole compositions in Xitieshan garnet-amphibolite and amphibolite samples.

Table 8.2 Representative microprobe analyses of amphibole. in: inclusion; c: core; r: rim; sym: symplectite; m: matrix amphibolite.

Sample	09NQ44				09NQ43				09NQ50				09NQ55			
Spot	3-in	1-sym	3-sym	5	4	3	6-c	6-r	1	1	3-r	3-c	1-c	1-r	1-c	1-r
Mineral	Ts	Act	Mg-hbl	Mg-hbl	Prg	Ed	Mg-hbl	Mg-hbl	Prg	Ed	Mg-hbl	Mg-hbl	Ed	Ed	Mg-hbl	Mg-hbl
SiO_2	43.8	53.96	46.29	46.19	42.85	43.10	44.50	46.62	42.19	43.37	45.17	46.79	42.97	42.80	46.75	45.30
TiO_2	0.81	0.11	0.56	0.75	0.95	0.90	0.91	0.64	0.87	0.78	0.50	0.32	0.91	0.89	0.71	0.85
Al_2O_3	13.0	2.31	10.09	10.46	13.32	12.58	11.00	8.96	13.77	12.55	10.19	8.63	12.35	12.61	9.02	9.77
FeO	16.3	10.13	15.45	15.09	14.88	14.77	14.91	15.20	14.51	15.91	14.87	14.95	16.00	15.90	15.59	16.54
MnO	0.17	0.00	0.17	0.15	0.31	0.31	0.33	0.32	0.29	0.33	0.31	0.33	0.32	0.34	0.30	0.28
MgO	10.3	20.13	12.01	11.76	9.74	9.92	10.58	11.31	9.83	9.73	11.19	11.84	9.58	9.48	11.17	10.46
CaO	11.9	13.02	11.87	12.18	11.45	11.61	11.64	11.64	11.61	11.76	11.37	11.30	11.51	11.65	11.66	11.68
Na_2O	1.58	0.17	1.06	1.27	1.28	1.26	1.16	0.88	1.15	1.09	0.86	0.65	1.31	1.24	1.12	1.20
K_2O	0.58	0.10	0.36	0.38	1.59	1.40	1.14	0.89	1.72	1.54	1.23	0.81	1.49	1.40	0.96	1.03
Total	98.6	99.94	97.87	98.23	96.37	95.84	96.16	96.45	95.94	97.07	95.68	95.62	96.43	96.31	97.28	97.10
Si	6.40	7.51	6.73	6.73	6.47	6.53	6.70	6.96	6.40	6.53	6.82	7.01	6.52	6.50	6.95	6.80
Al^{IV}	1.51	0.38	1.21	1.19	1.43	1.37	1.19	0.97	1.51	1.39	1.12	0.95	1.38	1.40	0.97	1.10
Al^{VI}	0.74	0.00	0.52	0.60	0.94	0.88	0.76	0.61	0.96	0.84	0.69	0.57	0.83	0.85	0.61	0.63
Ti	0.09	0.01	0.06	0.08	0.11	0.10	0.10	0.07	0.10	0.09	0.06	0.04	0.10	0.10	0.08	0.10
Mn	0.02	0.01	0.02	0.02	0.04	0.04	0.04	0.04	0.04	0.04	0.04	0.04	0.04	0.04	0.04	0.03
Mg	2.26	4.18	2.60	2.55	2.19	2.24	2.38	2.52	2.22	2.18	2.52	2.64	2.17	2.15	2.48	2.34
Ca	1.87	1.94	1.85	1.90	1.85	1.89	1.88	1.86	1.89	1.90	1.84	1.81	1.87	1.90	1.86	1.88
Na	0.45	0.05	0.30	0.36	0.38	0.37	0.34	0.25	0.34	0.32	0.25	0.19	0.38	0.37	0.32	0.35
K	0.11	0.02	0.07	0.07	0.31	0.27	0.22	0.17	0.33	0.30	0.24	0.15	0.29	0.27	0.18	0.20
Fe^{3+}	0.46	0.09	0.60	0.33	0.00	0.00	0.00	0.08	0.00	0.00	0.00	0.14	0.00	0.00	0.00	0.00
Fe^{2+}	1.53	1.09	1.28	1.51	1.88	1.87	1.88	1.82	1.84	2.00	1.88	1.73	2.03	2.02	1.94	2.08
Cations	15.4	15.27	15.23	15.34	15.58	15.56	15.49	15.35	15.61	15.58	15.46	15.29	15.61	15.59	15.43	15.51
K/Ca	0.06	0.01	0.04	0.04	0.17	0.14	0.12	0.09	0.18	0.16	0.13	0.09	0.15	0.14	0.10	0.11
Fe/Mn	100	118	94	92	47	47	47	48	46	50	47	47	51	51	49	69

Sample 09NQ43 is a fine-grained amphibolite, with a mineral assemblage comprising amphibole, feldspar, chlorite and minor titanite. The overall texture of the rock is granoblastic. Amphiboles (0.1 – 0.5 mm in grain size) are classified as pargasite, edenite and

magnesio- hornblende, with K_2O = 0.9 – 1.6 wt.%, K/Ca = 0.09 – 0.17 and Fe/Mn = 47 (19 points, Table 8.2). As present in Figure 8.2, amphiboles from the garnet amphibole are characterized by lower K/Ca but higher Fe/Mn ratios; whereas amphiboles from the amphibolite exhibit an opposite compositional trend. Feldspar has a general composition of $Ab_{54-85}An_{0-36}Or_{0-41}$ (Table 8.3).

Table 8.3 Representative microprobe analyses (wt.%) of feldspar (5 cations).

Sample	09NQ44		09NQ43			09NQ42	09NQ50	
Mineral	Fsp		Fsp			Kfs	Fsp	
Spot	1-sym	1-sym	1	1	1	2	1	7
SiO_2	54.95	56.22	63.16	58.82	61.66	64.04	56.80	40.44
TiO_2	0.00	0.00	0.01	0.00	0.01	0.04	0.01	0.08
Al_2O_3	27.58	27.27	22.01	25.00	22.74	19.14	27.16	25.30
FeO	0.07	0.07	0.11	0.28	0.23	0.31	0.03	4.82
MnO	0.00	0.00	0.00	0.00	0.03	0.01	0.00	0.11
MgO	0.02	0.01	0.13	0.15	0.21	0.17	0.00	0.02
CaO	9.51	8.92	1.47	4.41	0.39	0.04	8.56	26.40
Na_2O	5.75	6.26	9.31	5.78	6.05	0.28	6.29	0.07
K_2O	0.25	0.10	1.30	3.90	6.48	15.17	0.37	0.02
Total	98.12	98.84	97.50	98.34	97.81	99.19	99.22	97.26
Si	2.52	2.55	2.86	2.69	2.83	3.01	2.57	2.09
Al	1.49	1.46	1.17	1.35	1.23	1.06	1.45	1.55
Ca	0.47	0.43	0.07	0.22	0.02	0.00	0.41	1.35
Na	0.51	0.55	0.82	0.51	0.54	0.03	0.55	0.01
K	0.01	0.01	0.08	0.23	0.38	0.91	0.02	0.00
Cations	5.00	5.00	5.00	5.00	5.00	5.00	5.00	5.00
XAn	0.47	0.44	0.07	0.23	0.02	0.00	0.42	0.99
XAb	0.51	0.56	0.85	0.54	0.57	0.03	0.56	0.00
XOr	0.01	0.01	0.08	0.24	0.41	0.97	0.02	0.00

Sample 09NQ50 is a medium-grained amphibolite, which consists of amphibole, feldspar and minor titanite. Amphibole grains usually exhibit sieve texture, in which irregular fine-grained plagioclase crystals (<10 μm) are enclosed in coarse-grained amphibole. They are magnesio-hornblende, pargasite and edenite (Table 8.2) and have relatively higher K/Ca but lower Fe/Mn ratios when compared with the garnet amphiboles of sample 09NQ44 (Figure 8.2). Most feldspar is pure anorthite (An_{99-100}) with an average K_2O content of ~0.02 wt.% (7 points, Table 8.3). One measured plagioclase grain has a composition of $Ab_{67}An_{33}$ and K_2O = 0.04 wt.% (Table 8.3). Assuming local equilibrium between amphibole rims and adjacent plagioclase in amphibolites (09NQ43 and 50), the Amp-Pl geothermometer (Holland and Blundy, 1994) combined with the Amp-Pl-(Qz) geobarometer(Bhadra and Bhattacharya, 2007) gives a range of *P-T* conditions of 5.0 – 7.2 kbar and 530 – 630 °C, representing medium-pressure lower amphibolite-facies conditions.

Biotite schist 09NQ42 is mainly composed of biotite and feldspar with minor muscovite, amphibole and quartz. Biotite usually has straight grain boundaries with feldspar, with relatively high TiO_2 contents (2.75 – 2.97 wt.%, Table 8.4). It has a limited range of

compositions with Mg/(Mg + Fe_{total}) = 0.56. Feldspars are pure K-feldspar with a general composition of $Ab_0An_3Or_{97}$ (Table 8.4)

Table 8.4 Representative microprobe analyses (wt%) of muscovite (normalized to 11 O), biotite (normalized to 11 O), feldspar (5 cations). c:core; r: rim

Sample	09NQ51		09NQ52		09NQ55		09NQ42	Sample	09NQ50		09NQ51		09NQ52		09NQ55	
Mineral	Ms		Ms		Ms		Bt	Mineral	Pl	Pl	K-fsp	Pl	K-fsp	Pl	K-fsp	Pl
Spot	3-c	4-r	3-c	3-r	4-c	3-r	10	Spot	1	7	4	3	6	1	7	4
SiO_2	46.38	46.20	46.94	46.68	46.83	46.72	37.69	SiO_2	59.80	43.67	63.40	61.61	64.29	62.72	63.04	56.60
TiO_2	0.90	1.06	0.73	0.77	0.84	0.86	2.86	TiO_2	0.01	0.08	0.01	0.00	0.01	0.00	0.01	0.00
Al_2O_3	31.97	32.94	34.93	35.01	33.90	34.37	15.97	Al_2O_3	27.16	25.30	19.53	23.09	18.59	22.94	18.46	26.53
FeO	2.42	1.87	3.07	3.18	2.45	2.70	17.31	FeO	0.03	4.82	0.01	0.02	0.01	0.00	0.02	0.04
MnO	0.03	0.01	0.02	0.01	0.03	0.00	0.18	MnO	0.00	0.11	0.00	0.01	0.00	0.01	0.00	0.00
MgO	1.24	0.92	0.92	0.91	1.01	0.92	12.53	MgO	0.00	0.02	0.00	0.00	0.00	0.00	0.00	0.01
CaO	0.04	0.00	0.00	0.00	0.01	0.00	0.02	CaO	5.56	24.65	0.02	4.40	0.03	4.09	0.03	8.42
Na_2O	0.43	0.47	0.51	0.52	0.52	0.49	0.10	Na_2O	6.29	0.07	0.70	9.92	1.02	9.01	0.68	6.27
K_2O	10.43	10.69	10.07	9.63	10.12	10.03	9.73	K_2O	0.04	0.02	15.71	0.25	15.27	0.31	15.58	0.31
Total	93.82	94.17	97.20	96.72	95.71	96.09	96.36	Total	98.88	98.74	99.39	99.30	99.21	99.08	97.81	98.19
Si	3.16	3.13	3.08	3.07	3.12	3.10	2.81	Si	2.72	2.18	2.94	2.72	2.99	2.80	2.97	2.59
Al	2.56	2.63	2.70	2.72	2.66	2.68	1.41	Al	1.45	1.49	1.07	1.20	1.02	1.21	1.03	1.43
Ti	0.05	0.05	0.04	0.04	0.04	0.04	0.16	Ca	0.27	1.32	0.00	0.21	0.00	0.20	0.00	0.41
Fe_{total}	0.14	0.11	0.17	0.18	0.14	0.15	1.08	Na	0.55	0.01	0.06	0.85	0.09	0.78	0.06	0.56
Mn	0.00	0.00	0.00	0.00	0.00	0.00	0.01	K	0.00	0.00	0.93	0.01	0.90	0.02	0.94	0.02
Mg	0.13	0.09	0.09	0.09	0.10	0.09	1.39	Cations	5.00	5.00	5.00	5.00	5.00	5.00	5.00	5.00
Ca	0.00	0.00	0.00	0.00	0.00	0.00	0.00									
Na	0.06	0.06	0.07	0.07	0.07	0.06	0.01	XAn	0.33	0.99	0.00	0.19	0.00	0.20	0.00	0.42
K	0.91	0.92	0.84	0.81	0.86	0.85	0.93	XAb	0.67	0.00	0.06	0.79	0.09	0.79	0.06	0.56
Cations	7.00	7.00	6.99	6.97	6.98	6.97	7.80	XOr	0.00	0.00	0.94	0.01	0.91	0.02	0.94	0.02

Two medium-grained gneisses (09NQ51 and 09NQ52) contain similar assemblages of muscovite, feldspar, quartz and biotite. Accessory minerals are titanite and zircon. Slightly deformed, medium-grained muscovite (up to ~1.5 mm) usually grew along the main foliation and shows that there are no significant compositional differences between these two samples. Muscovite grains are internally homogenous in composition with Si contents of 3.08 –.3.16 p.f.u. in the cores and 3.07 –.3.13 p.f.u. in the rims (see Table 8.4). Feldspar mainly occurs as anhedral grains and forms two groups with generalized compositions of $Ab_{6-9}An_0Or_{91-94}$ and $Ab_{79}An_{19-20}Or_{1-2}$ (see Table 8.4).

Sample 09NQ55 is a medium-grained granitic gneiss, consisting of feldspar, quartz, biotite, amphibole and muscovite, with accessory titanite and zircon. Feldspar commonly occurs as subhedral to anhedral grains and can be divided into two groups with general compositions of $Ab_6An_0Or_{94}$ and $Ab_{56}An_{42}Or_2$ (Table 8.4). Amphibole is classified as edenite and K/Ca and Fe/Mn ratios are within the range of those of amphibole from the amphibolites (Figure 8.2). Fine-grained muscovite is generally associated with biotite, and has relatively homogeneous compositions within grains with Si contents of 3.12 p.f.u. in the cores and 3.10 p.f.u. in the rims (see Table 8.4).

8.4 ^{40}Ar/^{39}Ar results

The ^{40}Ar/^{39}Ar laser stepwise heating experiments of the amphiboles, muscovite and biotites were completed at the argon isotope laboratory in VU University Amsterdam. The K-feldspar ^{40}Ar/^{39}Ar measurements were carried out in the argon isotope laboratory in Guangzhou Institute of Geochemistry, Chinese Academy of Sciences (GIGCAS). The gas purification processes in Amsterdam and Guangzhou are different. In VU University, the released gases were purified by a Fe/V/Zr getter pump operated at 250 °C and a SAES NP10 Zr/Al pump operated at 450 °C. The purified gases were analyzed for the argon isotopes in a MAP 215-50 mass spectrometer. In GIGCAS, the gases were purified for 5 − 8 minutes in an ultrahigh vacuum line using Zr/Al getters and a cold trap kept at *ca.* - 90 °C. The purified gases were analyzed for the argon isotopes in a GV Instruments 5400® mass spectrometer. The experiments always began with the analysis of a system blank and subsequently blanks were measured after every four to six gas extraction steps.

The ^{40}Ar/^{39}Ar step heating data were calculated and plotted using the ArArCALC2.50 software package (Koppers, 2002) and summarized in Table 8.5. The ^{40}Ar/^{39}Ar analytical results are listed in Appendix B. Age spectra and inverse isochrons (^{36}Ar/^{40}Ar vs. ^{39}Ar/^{40}Ar) for each of the samples are plotted in Figure 8.3 through Figure 8.5. All plateau and inverse isochron age uncertainties are given at 2σ level.

Table 8.5 Sample locations and summary of new ^{40}Ar/^{39}Ar ages*

Sample	Mineral	TGA (Ma, 2σ)	WA (Ma, 2σ)	Step (Total)	$^{39}Ar_k$ (%)	IIA (Ma, 2σ)	^{40}Ar/^{36}Ar	MSWD (IIA)
09NQ43	Amp	449.6 ± 2.1	438.3 ± 5.5	7-16(19)	74.1	418.1 ± 2.7	686 ± 34	2.7
09NQ44	Amp	480.9 ± 2.3	468.5 ± 13.5	5-18(19)	91	425.1 ± 2.6	705 ± 14	2
09NQ50	Amp	439.5 ± 2.0	419.4 ± 1.9	8-15(17)	46.1	419.2 ± 2.0	317 ± 52	0.07
09NQ55	Amp	422.8 ± 1.9	419.8 ± 1.9	4-19(19)	92.2	419.7 ± 1.9	298 ± 18	1.1
09NQ51	Ms	409.1 ± 1.9	409.1 ± 1.9	2-15(15)	96.1	409.2 ± 1.9	282 ± 29	0.8
09NQ52	Ms	406.6 ± 1.8	407.6 ± 1.9	4-15(15)	87.2	407.4 ± 1.8	325 ± 27	0.7
09NQ55	Ms	407.3 ± 1.9	407.2 ± 1.9	1-14(14)	100	407.0 ± 1.8	308 ± 12	0.9
09NQ42	Bt	392.9 ± 1.9	396.3 ± 2.0	2-11(11)	89.1	396.5 ± 2.0	284 ± 32	1.5
09NQ51	Kfs	307.3 ± 2.9	320.5 ± 3.0	7-12(12)	38.9	320.4 ± 3.4	309 ± 132	0.3
09NQ52	Kfs	293.7 ± 2.7	314.5 ± 3.0	11-14(14)	16.4	314.0 ± 3.0	319 ± 39	0.04
09NQ55	Kfs	278.0 ± 2.6	294.3 ± 2.8	7-12(12)	33.5	294.0 ± 2.8	315 ± 38	0.2

*TGA: total gas age; WA: weighted age; IIA: inverse isochron age; MSWD: mean square weighted

8.4.1 Amphibole

Amphibole 09NQ44Amp was separated from the garnet amphibolite. The age spectrum by laser stepwise heating is characterized by monotonically decreasing, anomalously old apparent ages in the first few steps and significantly younger apparent ages in the final steps, with a total gas age of 480.9 ± 2.3 Ma (Figure 8.3a, Table 8.5). The K/Ca ratio of the analyzed amphibole, derived from interference-corrected $^{37}Ar_{Ca}/^{39}Ar_K$ ratio, is very constant after exclusion of the first step, demonstrating the high purity of the analyzed amphibole grains

(Figure 8.3a). In the isotope correlation diagram ($^{36}Ar/^{40}Ar$ vs. $^{39}Ar/^{40}Ar$), consecutive data points (steps 5 – 18) reveal a well-defined isochron with age of 425 ± 2.7 (MSWD = 2.0) and an initial $^{40}Ar/^{36}Ar$ ratio of 705 ± 13 (Figure 8.3b). This $^{40}Ar/^{36}Ar$ value is higher than that of the modern atmospheric air, implying the presence of extraneous argon (i.e., argon that is not produced by *in situ* radiogenic decay of ^{40}K) within amphibole. Applying this initial $^{40}Ar/^{36}Ar$ ratio to correct for the non-atmospheric/non-radiogenic ^{40}Ar component in the sample, the recalculated ages reveal a flat age spectrum with a plateau age of 425.1 ± 2.6 Ma for approximately 91% of the total ^{39}Ar released (Figure 8.3a).

Amphibole samples 09NQ43Amp and 09NQ50Amp were separated from amphibolites. Laser stepwise heating analyses on these two samples produced similar age spectra and isochron diagrams to those of 09NQ44Amp: (1) Monotonically decreasing release patterns with anomalously old apparent ages in the first few steps and significantly younger apparent ages of the last two or three steps (Figure 8.3c, e). (2) The K/Ca ratios of the two analyzed amphibole samples are very constant. The respective mean K/Ca values of 0.09 ± 0.02 (09NQ43) and 0.11 ± 0.01 (09NQ50) obtained from $^{40}Ar/^{39}Ar$ dating are within error of the ratios obtained by EMPA of 0.12 ± 0.04 and 0.13 ± 0.04 (Figure 8.3c, e; Table 8.2). (3) On the inverse isochron diagrams, regression of steps 7 – 16 and 5 – 18 yield ages of 418.1 ± 2.7 Ma and 418.8 ± 2.0 Ma with initial $^{40}Ar/^{36}Ar$ ratios equal to 686 ± 34 and 628 ± 39 for samples 09NQ43Amp (Figure 8.3d) and 09NQ50Amp (Figure 8.3f), respectively. As before, flat age spectra with plateau ages of 418.1 ± 2.2 Ma (Figure 8.3c) and 418.8 ± 2.0 Ma (Figure 8.3e) were obtained when ages were recalculated using the initial $^{40}Ar/^{36}Ar$ values from the isochrons for the corresponding steps.

Amphibole 09NQ55Amp was separated from an orthogneiss. Laser stepwise heating yielded a total gas age of 422.8 ± 1.9 Ma and showed older apparent ages for the first three steps (585 – 430 Ma), which account for ~8% of the cumulative ^{39}Ar released (Figure 8.3g). The remainder of the experiment produced younger and concordant apparent ages with a plateau age of 419.8 ± 1.9 Ma (taking about 92% of the total ^{39}Ar released, Figure 8.3g). The plateau portion from this sample exhibits a constant K/Ca ratio of 0.13 ± 0.01 (Figure 8.3g), which overlaps its EMPA K/Ca values of 0.1 – 0.15 (Table 8.2). The data points constituting the age plateau yield a well-defined isochron with an intercept age of 419.7 ± 2.0 (MSWD = 1.1) and an initial $^{40}Ar/^{36}Ar$ ratio of 298 ± 18 (Figure 8.3h), which indicates that there is little or no extraneous argon present in this sample.

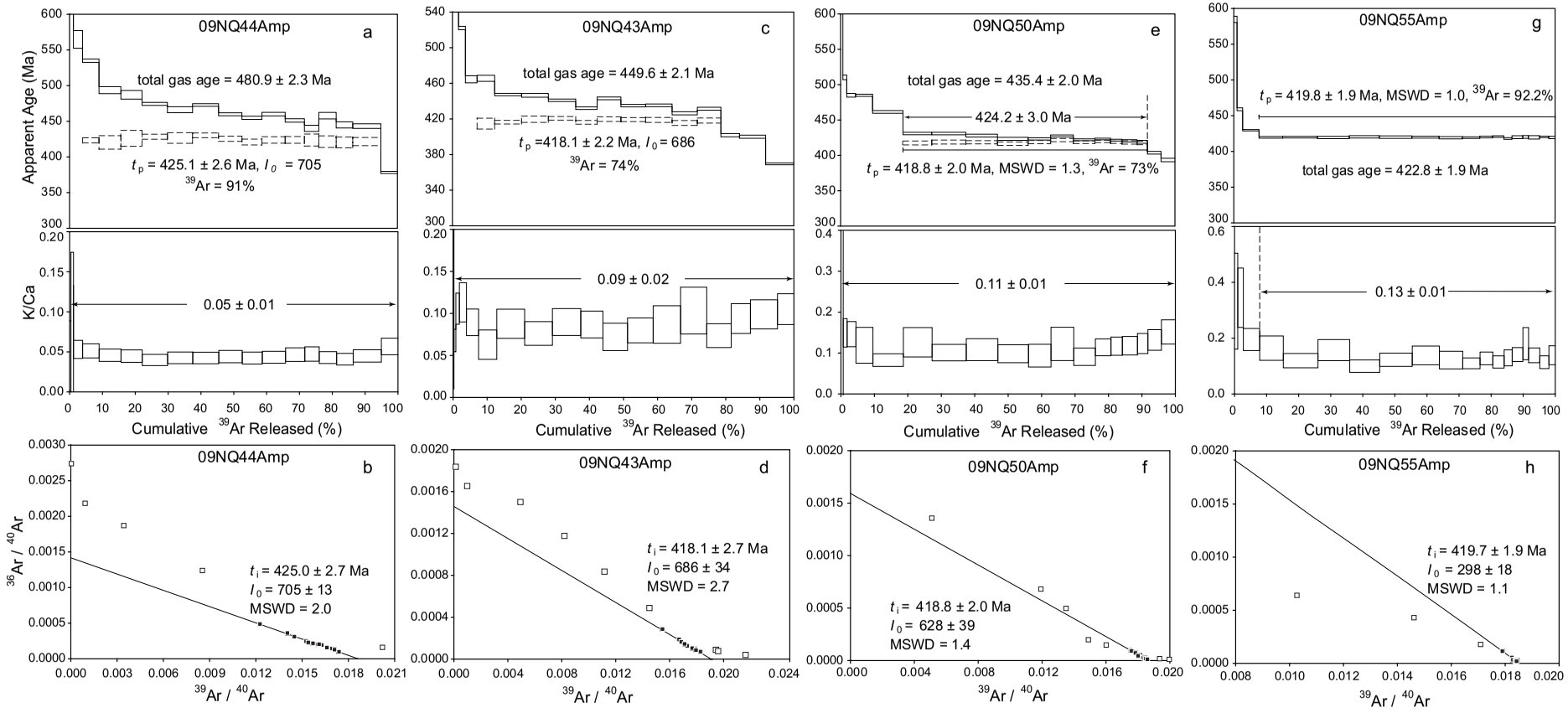

Figure 8.3 Apparent age spectra, K/Ca spectra, and inverse isochrons for amphiboles from the Xitieshan metamorphic rocks by laser stepwise heating. The older spectra (solid lines) were calculated assuming a trapped $^{40}Ar/^{36}Ar$ ratio of 295.5, while the spectra with younger ages (dash lines) were calculated using the indicated $^{40}Ar/^{36}Ar$ ratio (I_0). On the inverse isochrons, the green data points are included in the calculations of plateau and isochron ages, while the blue ones are excluded. Errors are quoted at the 2σ level.

8.4.2 Muscovite and Biotite

Muscovite was separated from the country-rock gneisses, and gave coherent and similar results when analysed by the $^{40}Ar/^{39}Ar$ method (Table 8.5; Figure 8.4).

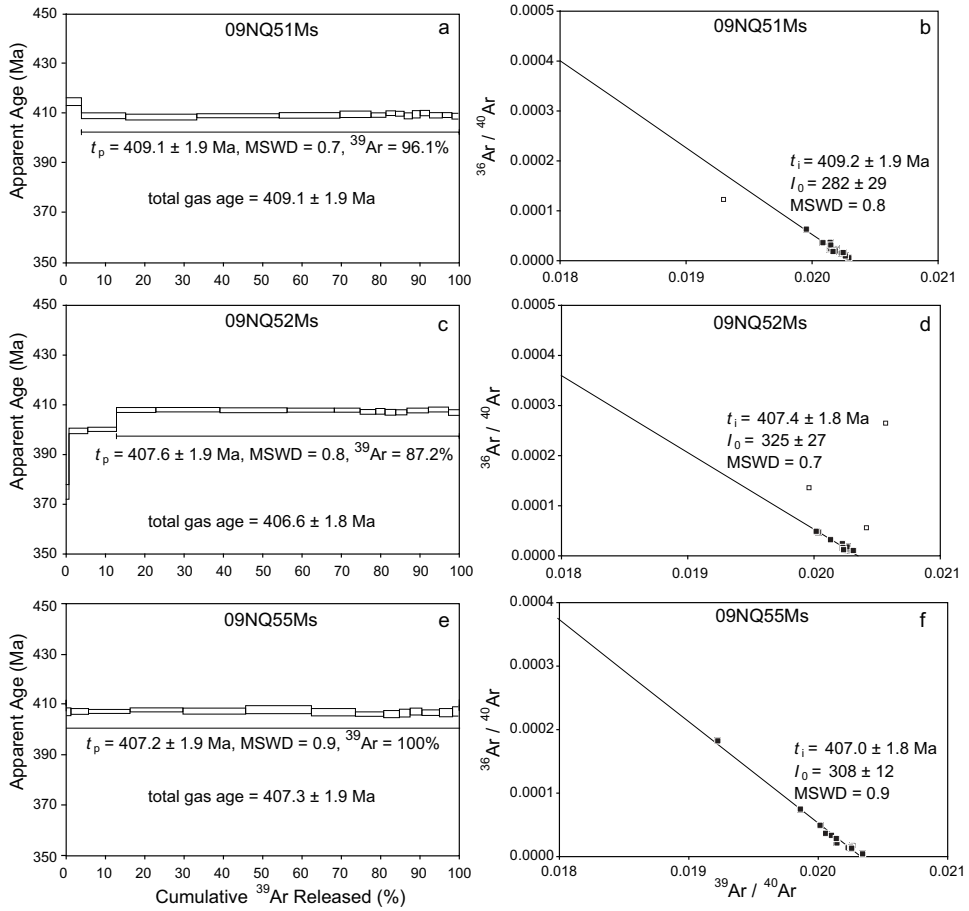

Figure 8.4 Apparent age spectra and inverse isochrons for muscovites from the Xitieshan gneisses by laser stepwise heating.

The age spectrum for 09NQ51Ms muscovite is characterized by one slightly old apparent age (ca. 415 Ma) in the first step and followed by a flat age spectrum with a plateau age of 409.1 ± 1.9 Ma (MSWD = 0.7, ^{39}Ar = 96%, Figure 8.4a). The inverse isochron defined an initial $^{40}Ar/^{36}Ar$ ratio of 282 ± 29, slightly less than, but still within error equal of the atmospheric value of 295.5, and an inverse isochron age of 409.2 ± 1.9 Ma (MSWD = 0.8, Figure 8.4b). Muscovite 09NQ52Ms produced younger apparent ages in the first three steps (375 – 400 Ma) and a flat age spectrum for the remainder of the experiment, giving plateau age of 407.6 ± 1.9 Ma (MSWD = 0.8, ^{39}Ar = 87%, Figure 8.4c). The data points contributing to the age plateau yielded a well-defined isochron with an inverse isochron age of 407.4 ± 1.8 Ma (MSWD = 0.7) and an initial $^{40}Ar/^{36}Ar$ ratio of 325 ± 27 (Figure 8.4d). Stepwise heating of muscovite 09NQ55Ms produced a perfectly flat age spectrum for all the steps with a plateau age of 407.2 ± 1.9 Ma (MSWD = 0.9, Figure 8.4e). The inverse isochron revealed an age of

407 ± 1.8 Ma (MSWD = 0.9) and an initial ^{40}Ar/^{36}Ar ratio of 308 ± 12 (Figure 8.4f).

Biotite 09NQ42Bt was separated from the schist. Laser stepwise heating yielded a younger apparent age of ca. 365 Ma in the first step and an age plateau with around 89% of the cumulative ^{39}Ar released at 396.3 ± 2 Ma (MSWD = 1.4, Figure 8.5a). The isotope correlation diagram yields an intercept age at 396.5 ± 2 Ma (MSWD = 1.5) and an initial ^{40}Ar/^{36}Ar ratio of 284 ± 32, which are consistent with the plateau age as well as the atmospheric value for the ^{40}Ar/^{36}Ar ratio (Figure 8.5b), respectively.

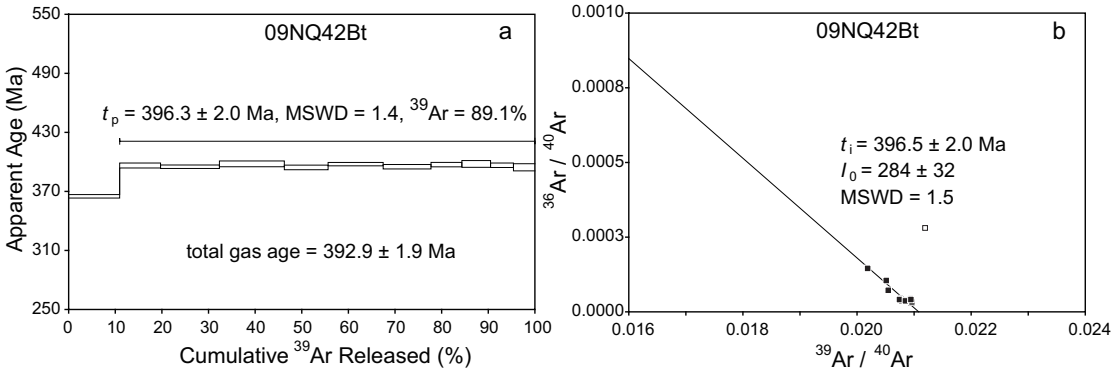

Figure 8.5 Apparent age spectrum and inverse isochron for biotite from the Xitieshan schist determined by laser stepwise heating.

8.4.3 K-feldspar

Potassic feldspar was obtained from the same gneisses from which we separated the muscovites. Laser stepwise heating of K-feldspar 09NQ51kfs produced an increasing staircase-shaped age spectrum with the youngest apparent ages in first three steps (ca. 280 Ma) and the oldest apparent ages (ca. 320 Ma) in the last segment (Figure 8.6a). A flat age spectrum with plateau age of 320.5 ± 3 Ma was obtained from the last six steps (MSWD = 0.3), which comprise 39% of the total ^{39}Ar released (Figure 8.6a). The data points that form the age plateau gave a concordant isochron age of 320.4 ± 3.4 Ma (MSWD = 0.34) and an initial ^{40}Ar/^{36}Ar ratio of 309 ± 132 (Figure 8.6b). It should be pointed out that the large error of the ^{40}Ar/^{36}Ar value is the result of the high radiogenic argon content of the plateau steps preventing the calculation of a precise non-radiogenic intercept value from the regression line. Laser stepwise heating of the other two K-feldspar separates 09NQ52kfs and 09NQ55kfs yielded similar increasing staircase-shaped release patterns. Sample 09NQ52kfs yielded a plateau age of 314.5 ± 3.0 Ma (MSWD = 0.2) by the last four steps with 16.4 of ^{39}Ar released (Figure 8.6c). A concordant isochron age of 314 ± 3 Ma (MSWD = 0.04) was obtained from the inverse isochron diagram with an initial ^{40}Ar/^{36}Ar ratio of 319 ± 39 (Figure 8.6d). Separate 09NQ55kfs produced a plateau age of 294.3 ± 2.8 Ma (MSWD = 0.2) in the last six steps with 34% of ^{39}Ar released (Figure 8.6e). A concordant isochron age of 294 ± 2.8 Ma (MSWD = 0.23) was obtained from the inverse isochron diagram with an initial ^{40}Ar/^{36}Ar ratio of 315 ± 38 (Figure 8.6ef).

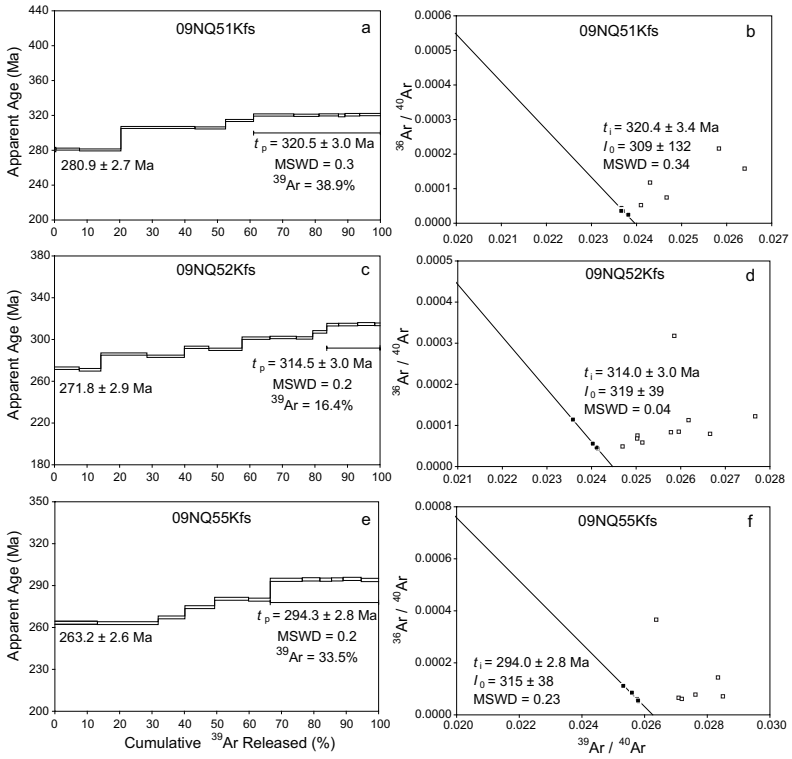

Figure 8.6 Apparent age spectra and inverse isochrons of K-feldspar separates from Xitieshan gneisses by laser stepwise heating.

8.5 Discussion

8.5.1 Relationships between lithology, mineral composition and $^{40}Ar/^{39}Ar$ data

Amphibole separates from mafic amphibolites (09NQ43, 44 and 50) and gneiss (09NQ55) have been dated by $^{40}Ar/^{39}Ar$ stepwise heating and analysed chemically by electron microprobe analyses. Based on the features of release spectra and age results, consistent relationships of ages with lithology and mineral compositions become apparent:

(1) Amphibole samples from the garnet-amphibolite and amphibolites yielded similar monotonically declining staircase-shaped release patterns, which are marked by anomalously older apparent ages at low temperature steps (Figure 8.3a, c and e). In contrast, amphibole from the granitic gneiss yields a flat age spectrum despite older apparent ages in the initial steps (Figure 8.3g).

(2) On the isotope correlation diagrams, a series data points of amphiboles from the garnet-amphibolite and amphibolites form well-defined isochrons with ages from 425 to 419 Ma and initial $^{40}Ar/^{36}Ar$ ratios of 628 – 705 (Figure 8.3b, d and f), suggesting the presence of extraneous ^{40}Ar (i.e. inherited or excess ^{40}Ar). Gneiss amphibole gives an isochron age of ca. 419 Ma and a $^{40}Ar/^{36}Ar$ composition indistinguishable from atmospheric (Figure 8.3h), precluding the presence of extraneous ^{40}Ar. Extraneous ^{40}Ar was identified in the mafic amphibolites whereas their felsic country rocks apparently did not retain the extraneous

argon. This difference in argon retentivity may due to their distinct lithology, bulk compositions and density of schistosity (Heinrich, 1982; Li et al., 1999; Baxter et al., 2002; Warren et al., 2011). In other words, under (U)HP conditions, extraneous ^{40}Ar was trapped in dense, less permeable rock like mafic eclogites, while at the same time from the more permeable rock types, like pelite and gneiss, the extraneous ^{40}Ar may have escaped more readily (Warren et al., 2012a; 2012b; Smye et al., 2013).

(3) The amphibole sample from the garnet-amphibolite yielded an isochron age of *ca.* 425 Ma, and was characterized by lower K/Ca but higher Fe/Mn ratios; whereas amphibole from the amphibolites and gneiss yield isochron ages of ca. 419 Ma and exhibit an opposite compositional trend (Figure 8.2). The composition differences may influence the Ar retentivity of the amphiboles that were separated from the different rock types (Onstott and Peacock, 1987; Dahl, 1996).

Different from amphibole, muscovite from the country rock gneisses does not show an obvious relationship between lithology, mineral composition and ^{40}Ar/^{39}Ar dating results. Although gneisses 09NQ51 and 09NQ52 has slightly different mineral assemblages and significantly larger grain size in comparison with sample 09NQ55 (see Table 8.4), their mineral compositions and ^{40}Ar/^{39}Ar plateau ages (Figure 8.4, left) are indistinguishable.

8.5.2 The possible sources of extraneous ^{40}Ar in amphibole

Extraneous ^{40}Ar is ubiquitous in the HP/UHP metamorphic rocks and is usually identified by the release patterns in age spectra (e.g., U- or saddle-shaped) or by anomalously old apparent ages (Hacker and Wang, 1995; Di Vincenzo and Palmeri, 2001), or by using additional dating methods such as Rb/Sr dating and ^{40}Ar/^{39}Ar dating on the same sample (Tonarini et al., 1993; Li et al., 1994; 1999; Sherlock et al., 1999; El-Shazly et al., 2001). In this study, the existence of extraneous ^{40}Ar in amphibole separates from garnet amphibolite and amphibolites was demonstrated by applying the laser stepwise heating ^{40}Ar/^{39}Ar method. The extraneous ^{40}Ar in amphibole could come from two sources: First, extraneous ^{40}Ar in amphibole could be derived from the UHP eclogite and its protolith. In particular, in the process of continental subduction, the gas activity is limited during “dry” UHP metamorphism (Arnaud and Kelley, 1995; Ruffet et al., 1995; Scaillet, 1996; Jahn et al., 2001; Smye et al., 2013). Therefore, part of the radiogenic argon could be probably kept in the eclogite as inherited argon (Wan and Chen, 1984; Di Vincenzo et al., 2001; Warren et al., 2012a; 2012b; 2012c). A series of retrograde metamorphic mineral assemblages formed during exhumation from deep to shallow. In the lower crust, amphibolite facies metamorphism began in a relatively closed system condition and part of the argon degassing deep sources (including from the eclogite) was trapped into the newly growing minerals of retrogressed eclogite equivalents, resulting in the extraneous ^{40}Ar found in amphiboles with initial ^{40}Ar/^{36}Ar ratios significantly higher than modern air ^{40}Ar/^{36}Ar ratios. This suggests that the extraneous ^{40}Ar in amphibole was derived from an internal origin and is due to incorporation of argon derived the local argon degassing activity.

Lower crust and upper mantle degassing may form an alternative source of extraneous ^{40}Ar within the amphiboles. The gas can be entrapped in the crystallizing amphibole through contamination and exchange interaction, most probably in fluid inclusions (Blanckenburg and Villa, 1988; Cumbest et al., 1994; Qiu et al., 2010). The very fine fluid inclusions with extraneous ^{40}Ar might be cracked in the high temperature steps during stepwise heating.

Unfortunately, the current data are not sufficient to address the exact sources of extraneous argon in amphibole. Additional work, such as oxygen and hydrogen isotopic analyses and $^{40}Ar/^{39}Ar$ *in vacuo* crushing analyses would probably help resolve these questions.

8.5.3 Interpretation of the new $^{40}Ar/^{39}Ar$ ages

The most striking finding of this study is that the $^{40}Ar/^{39}Ar$ data of amphiboles from the same area define an interval of ~6 Myr is characterized by a correlation between degree of retrograde overprinting and isotopic age: the stronger the amphibole retrogression, the younger the age. A similar trend has been discovered in other HP/UHP metamorphic belts (Di Vincenzo and Palmeri, 2001; Wilke et al., 2010). The Xitieshan samples were collected from a restricted area of less than 400 m^2. Thus, the explanation that the ages of amphiboles span an interval of ~6 Myr because the samples experienced a different thermal history can be excluded.

On the other hand, thermobarometric data in this study of the garnet-amphibolite and amphibolites from Xitieshan terrane reveal that the formation of calcic amphiboles (Amp-III) at 650 ± 20 °C and 8.6 ± 0.5 kbar, 580 ± 50 °C and 6.1 ± 1.1 kbar, respectively, represent different stages of retrograde metamorphism. Therefore, amphiboles are likely to have formed at different crustal depths and metamorphic conditions at different times during exhumation. This means that the growth of compositionally different amphiboles during eclogite retrogression was diachronous.

In general, the closure temperature for amphibole is assumed to be about 500 ± 50 °C for moderate cooling rates (Harrison, 1982; Dahl, 1996). Nevertheless, metamorphic amphiboles with higher "closure temperatures", even exceeding 650 °C, under particular circumstances like relatively fast cooling rates (> 10 °C/Myr), limited fluid circulation and high pressure have also has been proposed (Berger and York, 1981; Villa, 1998; Di Vincenzo and Palmeri, 2001; Wilke et al., 2010). Geothermometry on rocks from Xitieshan terrane suggests that the calcic amphiboles (Amp-III) in garnet-amphibolite equilibrated at 650 ± 20 °C, which overlaps the possible maximum closure temperature of metamorphic amphiboles. For this reason, the older isochron age of *ca.* 425 Ma from the garnet-amphibolite could be interpreted as a minimum estimate for the age of upper amphibolite-facies retrogression (P = 8.6 ± 0.5 kbar). On the other hand, the growth conditions of calcic amphiboles in Xitieshan amphibolites was estimated to be 580 ± 50 °C, which is closer to the regular closure temperature of amphibole. Therefore, the younger isochron ages of *ca.* 419 Ma from the Xitieshan amphibolites could be interpreted as cooling ages representing the timing of the

second stage of amphibole growth during lower amphibolite-facies metamorphism (P = 6.1 ± 1.1 kbar).

The Xitieshan gneiss samples record ^{40}Ar/^{39}Ar muscovite plateau ages from 407 to 409 Ma. Biotite from a schist yields a ^{40}Ar/^{39}Ar age plateau of ~396 Ma. These data agree with the argon plateau age of 405 Ma for a muscovite from monolithic gneiss reported by (Xu et al., 2006). Muscovite and biotite ages from country rocks that are systematically younger than the coexisting amphibole ^{40}Ar/^{39}Ar age (~418 Ma) from this study and the zircon U-Pb ages (422 – 460 Ma) previously reported by Zhang et al. (2009c) and Zhang et al. (2012), suggesting that extraneous argon is not present in the country rocks. In other words, these flat plateau spectra are reliable and not produced by data that contain homogeneously distributed extraneous ^{40}Ar.

The mineral assemblages, compositions of minerals and mineralogical thermometric data indicate that the host gneisses within the Xitieshan area were metamorphosed at P = 6.7 – 8.6 kbar and T = 705 – 800 °C, representing medium-pressure granulite metamorphism (Zhang et al., 2008a). This temperature vastly exceeds those at which muscovite/biotite becomes open to argon diffusion (Villa, 1998). Thus the muscovite and biotite ages from gneisses are interpreted to represent the time of cooling from peak metamorphic conditions through their closure temperatures, rather than the timing of crystallization. Particularly, the ^{40}Ar/^{39}Ar ages from the country rocks suggest that the Xitieshan terrane cooling below the assumed closure temperatures of muscovite (450 ± 25 °C, Villa, 1998; Harrison et al., 2009) and biotite (350 ± 25 °C, Harrison et al., 1985; Villa, 1998) occurred about 409 Ma and 396 Ma, respectively.

All K-feldspar samples yield gradually increasing release profiles in the early steps and concordant apparent ages in the later segment (Figure 8.6, left). The release patterns and younger apparent ages in the 263 – 286 Ma range during low temperatures indicate that these UHP rocks may have experienced diffusional Ar loss, probably resulting from plutonism (Wu et al., 2009a) or a regional ductile tectonic event (Rieser et al., 2006) during the middle-Permian. As before, the plateau ages in the 294 – 321 Ma range for the high temperature steps are regarded cooling ages (250 ± 25 °C, Heizler et al., 1988; McDougall and Harrison, 1999).

8.5.4 Exhumation rates and processes

In Xitieshan terrane, eclogites and their country gneisses show an "*in situ*" rather than "tectonic" relationship, which means that they shared the same tectono-metamorphic evolution, at least from UHP metamorphism onward (Zhang et al., 2006; Zhang et al., 2012). For this reason, the ^{40}Ar/^{39}Ar ages from the country rocks will also be used to constrain the *P-T-t* path of the mafic eclogites with corresponding closure temperatures and formation levels. Specifically, the data points were plotted using estimates for argon diffusion closure temperatures of 450 ± 25 °C for muscovite, 350 ± 25 °C for biotite and 250 ± 25 °C for K-feldspar. Pressure to depth conversion is calculated according to an assumed layered

lithosphere model and lithostatic pressure (Hodges, 1991; Rubatto and Hermann, 2001): a 20 km-thick upper crust and a 10 km-thick lower crust underlain by upper mantle with assumed densities of 2.7, 3.0 and 3.3 g/cm^3, respectively. The geothermal gradient of the upper crust is assumed to be 35 °C/km.

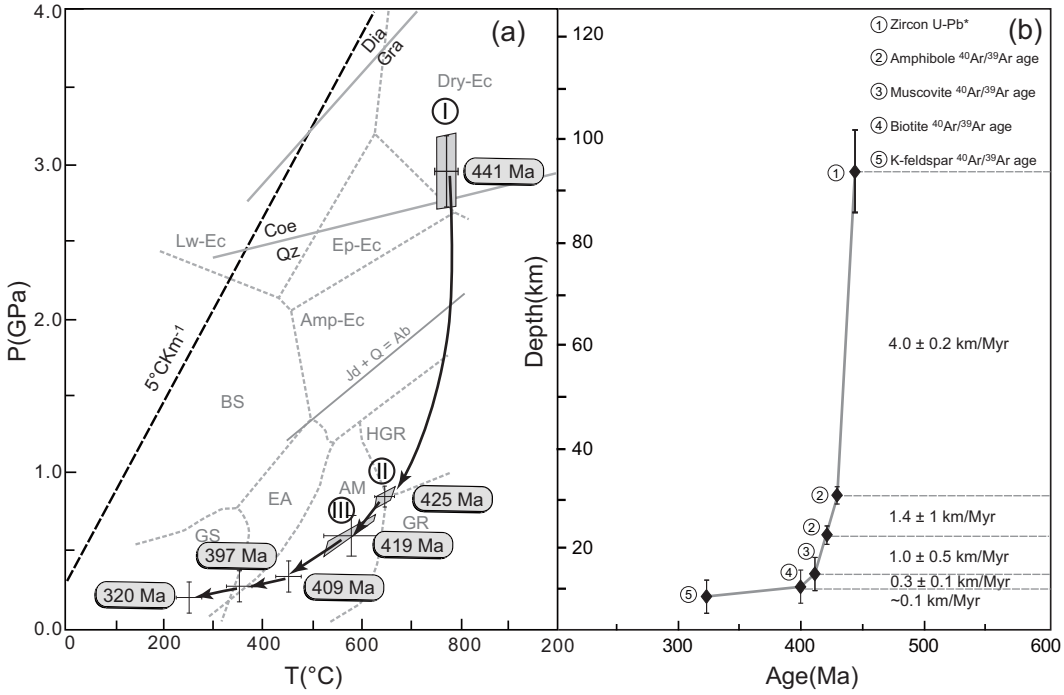

Figure 8.7 (a) Simplified *P-T-t* path of the Xitieshan UHP terrane. Peak eclogite-facies (I) *P-T* conditions from Zhang et al. (2011a). Retrograde granulite-facies (II) *P-T* conditions were obtained from garnet-amphibolite by using amphibole-plagioclase thermometry (Holland and Blundy, 1994) conbined with amphibole-plagioclase-(Qz) barometry (Bhadra and Bhattacharya, 2007). Amphibolite-facies (III) *P-T* conditions were obtained from amphibolites by applying amphibole-plagioclase thermometry (Holland and Blundy, 1994) conbined with amphibole-plagioclase-(Qz) barometry (Bhadra and Bhattacharya, 2007). (b) plot of depth *vs.* time (*z-t*) with exhumation volecities. The error bars on the age are too small to be shown.* zircon U-Pb age from Liu et al. (2012), ^{40}Ar/^{39}Ar ages from this study.

The peak metamorphic *P-T* conditions were estimated to be at 770 ± 20 °C and 29 ± 2 kbar by Zhang et al. (2011a), corresponding to ~95 km depth. The upper amphibolite-facies and lower amphibolite-facies metamorphic *P-T* conditions were calculated to at 650 ± 20 °C, 8.6 ± 0.5 kbar and 580 ± 50 °C, 6.1 ± 1.1 kbar (from this study), equivalent to ~31 and ~22 km depth. The burial depths derived from the assumed closure temperatures of muscovite, biotite and K-feldspar are ~13, ~10 and ~7 km, respectively. Based on the above *P-T* conditions, the new ^{40}Ar/^{39}Ar ages and zircon U-Pb data reported by Liu et al. (2012), a *P-T-t* path for retrograde metamorphism of the Xitieshan eclogite can be constructed.

As illustrated in Figure 8.7, after peak metamorphism, the UHP rocks in Xitieshan terrane were exhumed at a velocity of 4.1 ± 0.2 km/Myr from the upper mantle (~95 km at

about ~441 Ma) to the lower crust (~31 km at about ~425 Ma). From ~31 km to 13 km, the exhumation velocity decreases to ~1.4 – 1.0 km/Myr, and finally to less than ~0.3 km/Myr to the upper crust, about 7 km in depth (Figure 8.7b). Exhumation velocity in the first stage is much faster than the final stages when the tectonic units get close to the surface, which suggests a change of the exhumation mechanism. The initial rapid exhumation may be due to the buoyancy of the subducted slice caused by its relatively low density relative to the surrounding mantle (Davies and von Blanckenburg, 1995). In contrast, the final stages of exhumation are probably governed by extension and/or erosion (Platt, 1993; Warren, 2013).

8.6 Conclusions

1. The Xitieshan eclogite experienced prolonged amphibolite-facies retrogression, which resulted in diachronous amphibole formation at different crustal levels and *P-T* conditions during Paleozoic exhumation.
2. Amphiboles from garnet-amphibolite and amphibolites yield similar disturbed release patterns by ^{40}Ar/^{39}Ar age spectrum dating and are marked by anomalously old apparent ages in the initial steps, indicating the presence of extraneous ^{40}Ar. Their isochron ages of *ca.* 425 Ma and *ca.* 419 Ma are used to constrain the timing of medium pressure granulite-facies and low pressure amphibolite-facies metamorphic episodes.
3. Muscovite, biotite and K-feldspar from the country rocks are not contaminated by extraneous ^{40}Ar. Their respective ages of ~ 409, 397 and ~280 – 320 Ma are interpreted as cooling ages.
4. The *P-T-t* path reveals that the Xitieshan UHP rocks were exhumed quickly from ~95 km to ~31 km with a mean exhumation rate of ~4.0 km/Myr, whereas the subsequent exhumation to the upper crust proceeded at gentle rates of 1.4 – 0.1 km/Myr. Rapid initial exhumation may have been driven by buoyancy forces, while the subsequent slow uplift was probably caused by erosion and lithospheric extension.